Analysis of a Thin-Walled Pressurized Torus in Contact with a Plane

Michael J. Mack Jr.*
Hewlett-Packard Company, Fort Collins, Colorado
Paul M. Gassman†
Fisher Controls Company, Marshalltown, Iowa
and
Joseph R. Baumgarten‡
Iowa State University, Ames, Iowa

Finite element analysis is applied to study the large deflection of a standing torus loaded by a plane. The internally pressurized thin-walled structure is found to have an elliptical footprint area. Considerable bulge occurs in the sidewall in the region of the load plane. Stress distributions throughout the torus are shown for various load levels and for various modeling strategies at a given load level. In large load ranges finite element calculations show compressive circumferential stress and negative curvature in the footprint region. Results are compared with inelastic wall analysis.

Nomenclature

A = contact area, m^2
a = major torus radius, m
b = minor torus radius, m
L = load, N
P_a = atmospheric pressure, Pascal
P_i = initial torus gas pressure, Pascal
V = final torus volume, m^3
δ = torus deflection, m

Introduction

AIRCRAFT tires have been a subject of broad interest because of their importance to safe air travel. The aircraft tires carry the weight of the vehicle, provide the braking force in landing, and contribute significantly to the dynamics of the landing system.

Through the years, the primary research on aircraft tires has been empirical work where the relationships of load, deflection, and contact area have been observed. Smiley and Horne[1] developed dimensionless curves relating the contact area or footprint dimensions, pressure rise, and vertical deflection vs load for static aircraft tires. Clark[2] noted that the footprint area for aircraft tires is elliptical in shape which is associated with a toroidal carcass with little external tread or shoulder region. Van Eldik Thieme[3] stated that the tire stiffness was composed of a relatively constant part provided by the sidewall bending rigidity and partly by the internal pressure over the contact area. In aircraft tires, the bending rigidity accounts for about 3 to 8% of the total tire stiffness compared to 15% for automobile tires.

Since the bending contribution is small, and the tire stiffness results primarily from membrane stresses, a logical simplification for experiments and analysis might be the representation of an aircraft tire by an inner tube on a rim. De Eskinazi et al.[4] compared experimental results of deflection and footprint area vs load from an inner tube on a rim with results from a finite element computer program. The finite element program uses triangular, flat, membrane elements with linear interpolation functions to model the inner tube problem.

The analysis presented here will contain three distinct thrusts. First, a coarse analytical approximation that relates load to vertical deflection and contact area for a thin-walled toroidal structure will be developed. Second, an experimental apparatus that loads an inner tube on a rim will be utilized to provide experimental results for the toroidal structure problem. Last, a finite element program will be used to predict vertical deflections vs load and describe the stress distribution throughout the torus. The influence of decreasing the element grid size and the exploitation of symmetry will be considered in the finite element analysis. Examination of the resulting stresses under increasing load provides insight into the behavior of tires.

Analytical Approach

Analytical work has proceeded very slowly for aircraft tires due to difficulties in analyzing large deflections in toroidal shells and due to unsymmetric boundary conditions which develop from the contact of a tire with the ground. Jordan[5] developed a nonlinear membrane theory to solve the problem of a thin-walled torus loaded only by internal pressure. The analytic complexity increases when the contact of the torus with a plane is considered. As a result of the problem complexities, some assumptions and simplifications must be made to obtain an analytic approximation.

The analytical approach utilizes static force analysis and invokes Boyle's ideal gas law for isothermal gas compression. The geometries of the initial and final configurations provide estimates of the torus volumes and allow the internal pressures to be related. The analysis assumes that the inner tube walls are inelastic, nonstretching, and have no flexural rigidity. Furthermore, the volume contribution of the bulge region at the base of the tire is ignored to simplify the geometry of the deformed torus. A detailed derivation of the analysis may be found in Ref. 6.

Figure 1 shows the initial undeformed torus used in the analysis with the dimensions labeled. Equations (A1-A3) in the Appendix relate the initial dimensions, pressures, and load

Presented as Paper 82-0702 at the AIAA/ASME/ASCE/AHS 23rd Structures, Structural Dynamics, and Materials Conference, New Orleans, La., May 10-12, 1982; submitted May 12, 1982; revision received Nov. 16, 1982.

*Research Engineer.
†Structural Engineer.
‡Professor, Department of Mechanical Engineering.

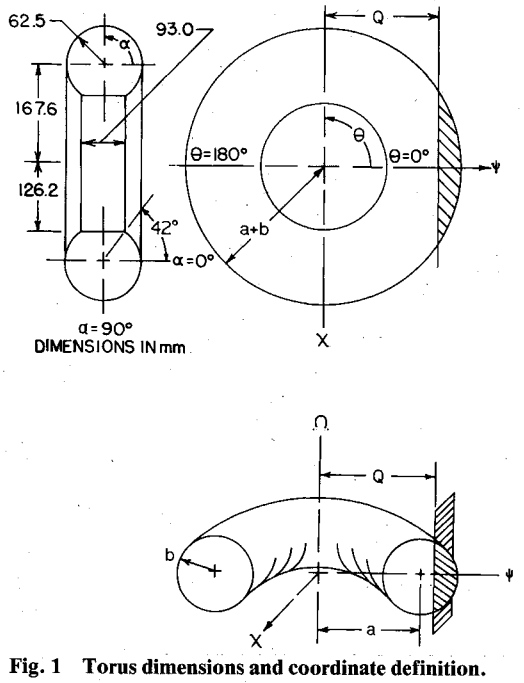

Fig. 1 Torus dimensions and coordinate definition.

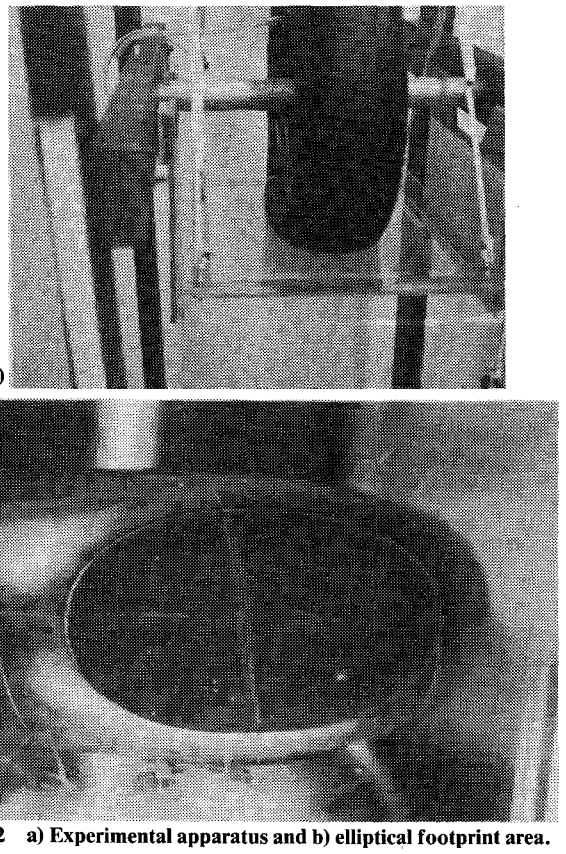

Fig. 2 a) Experimental apparatus and b) elliptical footprint area.

to the resulting vertical deflection of the torus. A computer program which uses a Regula Falsi technique to solve the equations for the deflection is listed in Ref. 6. Once the deflection has been estimated, the contact area may be calculated by Eq. (A4) of the Appendix.

Experimental Approach

An experimental apparatus provides a basis of comparison for the analytic approximation and for the finite element solution. An 0.2032×0.508-m Goodyear rubber inner tube was mounted on a steel rim. The rim was rigidly constrained

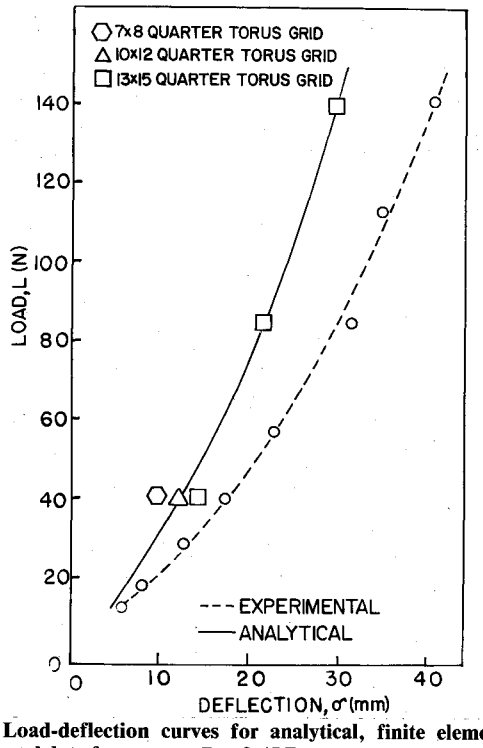

Fig. 3 Load-deflection curves for analytical, finite element, and experimental data for torus at $P_i = 3.45$ Pa.

to prevent deflection or rotation. Contact of a tire with a flat surface was simulated by vertically impinging a transparent plate onto the surface of the tube as shown in Fig. 2a. The transparent plate allowed the elliptical footprint area to be viewed as shown in Fig. 2b.

Experiments were conducted for three initial inflation pressures. Data from the experiments include the vertical loads applied by the plate, initial pressures, changes in pressures, and vertical deflections. Also, the major and minor diameters of the elliptical footprint were measured to determine the contact area.

Results of the Analytic and Experimental Approaches

Figure 3 shows the load-deflection curves resulting from the approximate analysis and from the experiments at an initial inflation pressure of 3.45 Pa. The prediction of deflections at a given load shows reasonable agreement, particularly at low loads. However, the stiffness of the torus has been overestimated at all loads. This overestimation results from the simplifications made in the analysis. Assuming non-stretching walls causes the stiffness to be overestimated. The assumption that the bulge region does not contribute to the final volume causes an even greater error in overestimating the stiffness, especially at high loads.

Finite Element Approach

Some of the difficulties encountered in an analytic formulation of this problem can be overcome in a finite element approach. The finite element method is generally advantageous when the geometry of the structure is irregular and the boundary or loading conditions are arbitrary. Consequently, the bulging in the sidewall and the unsymmetric loading conditions present no difficulty here.

The structural analysis of general shells (STAGS) computer code has been chosen for this finite element analysis because of the generality it provides in order to make comparisons of modeling strategies. A detailed discussion of this analysis is found in Ref. 7.

Summary of the Theory

STAGS uses a first-order shell theory to reduce a three-dimensional structural problem to a dependence upon two

spatial coordinates. As a result of the shell theory used, the rotations of the elements must be less than about 0.3 rad and the strains must be less than 0.1 to maintain good accuracy.

The elements selected for this analysis are rectangular plate elements where the geometry of the shell is constructed in a faceted form. Four corner nodes are used for each element. There are six degrees of freedom per node, three translation and three rotation. Displacement compatibility is enforced at the element boundaries by a combination of linear and cubic interpolation functions.

The kinematic relations include higher order terms to account for out of plane contributions to strain. The constitutive matrix includes both membrane and flexural components to improve the generality of the analysis, based on results found in Ref. 4.

A variational approach is used to derive the element equations where the principle of minimum potential energy is invoked. Numerical integration is employed to evaluate the element equations.

The nonlinear analysis uses an incremental loading procedure which allows the geometry and the structural stiffness characteristics to be updated at each load step. A Newton-like technique solves the system of nonlinear algebraic equations.

Modeling of Footprint Region

Because examination of various modeling options available in the STAGS code was of paramount interest, it was determined that utilizing experimental results in the footprint region would allow for the most accurate assessment of boundary condition selections. Based on the footprint area experimentally obtained for a given normal load, those nodes which would lie in the region were determined.

Once the nodes in the footprint region had been identified, the contact plane was imposed upon the torus by the application of a uniform force distribution over these nodes. The force imposed was divided proportionally among the nodes so that all interior nodes shared equally in the load while those nodes lying on the common boundary were given half the force loading of the interior ones. Because a quarter torus was used to model the tire, the node representing the centerpoint (or apex) of the footprint region was given only one-quarter of the interior nodal force in order to maintain the symmetry of the model.

Although utilization of experimental data to determine the contact region does not allow direct confrontation of the contact problem, it does allow for the refinement of boundary conditions and material modeling strategy within the STAGS code. Once this stratagem is refined adequately its position may serve as a guidepost from which refinement of the footprint region may be undertaken. Techniques have now been developed to bypass the experimental determination of footprint area. Iterative techniques produce the description of loaded nodes.

Results of the Finite Element Analysis

Figure 3 shows points on the load-deflection curve obtained by a 13×15 quarter torus grid at loads equal to 34.25, 69.84, and 114.32 N. The deflections predicted by the finite element solution are somewhat less than the experimental deflections. These smaller deflections result because STAGS is based on a minimum potential energy principle where the structural stiffness is overestimated with a coarse grid. As the grid size is refined, one would expect that the experimental solution would be approached with increasing deflections. At a load of 34.25 N, three different grid sizes are modeled. As the grid size is refined, the predicted deflection increases and approaches the experimental value.

In the course of the finite element analysis, the influence of some modeling parameters became clear. The influence of geometric nonlinearities and the use of an incremental loading procedure was very important. At 34.25-N load, a nonlinear analysis yielded a deflection of 84% of the experimental deflection while a linear analysis yielded a deflection of only 21% of the experimental value.

The description of the material properties of rubber to be used in the constitutive relations was another concern. Since the ingredients and treatments for rubber vary widely, Young's modulus of elasticity varies widely and the stress-strain relationship may be nonlinear. Tensile specimens of rubber were obtained from an inner tube identical to the one used in the experiments. The tensile tests indicated that the material was isotropic, slightly nonlinear, and that a reasonable value for Young's modulus was 1.779×10^6 Pa. A Poisson's ratio of 0.48 was used since the material was assumed to be incompressible. STAGS analyses were completed with both linear and nonlinear material descriptions for the rubber. The results indicated that there was almost no difference in predicted deflections or stress distributions between the linear or nonlinear material description. Therefore, for the level of strains observed, a linear material description was adequate.

Another important modeling consideration was the exploitation of symmetry. Figure 3 showed that as the grid size was refined, the finite element solution improved. However, refining the grid size increases the number of degrees of freedom in the system and may dramatically increase the amount of required computer storage and run time. Since a static torus has symmetry with respect to two axes, a quarter torus may be defined which improves the refinement of the

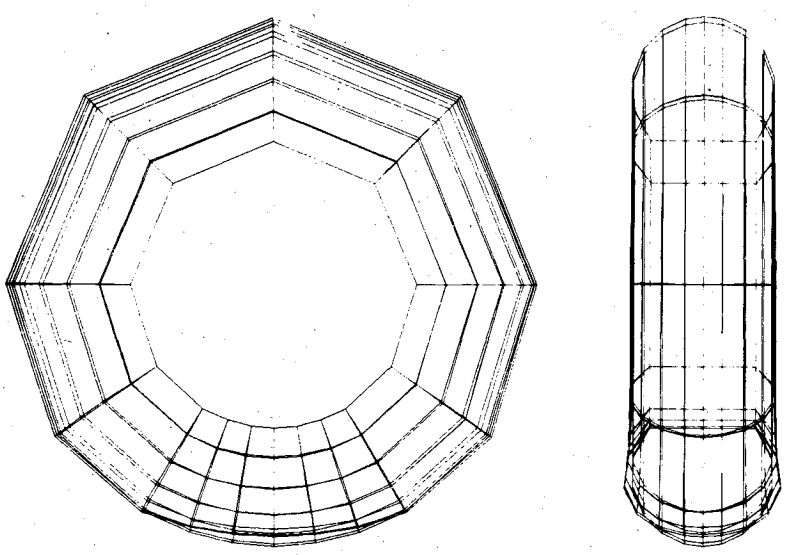

Fig. 4 A 13×15 full torus grid with 34.25-N load.

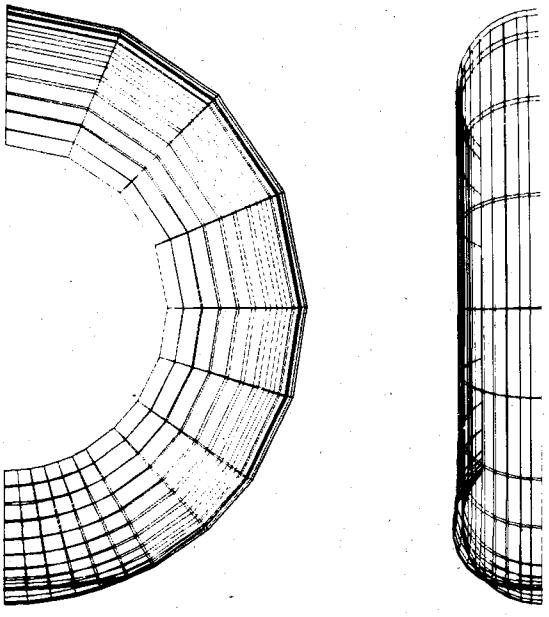

Fig. 5 A 13 × 15 quarter torus grid with 34.25-N load.

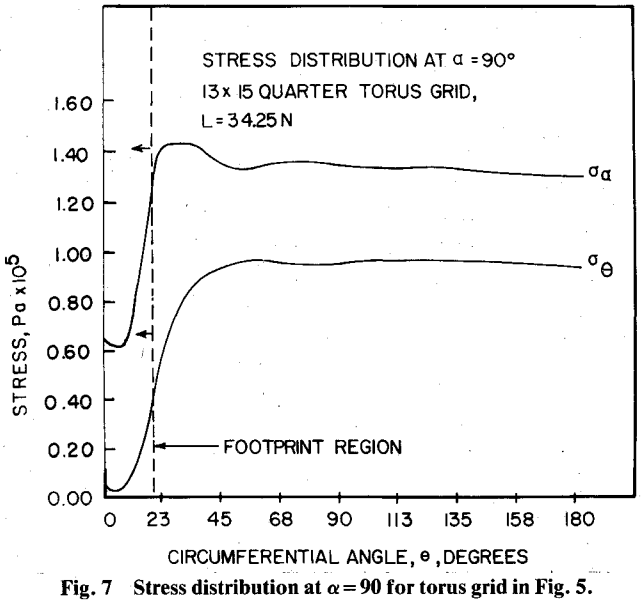

Fig. 7 Stress distribution at $\alpha = 90$ for torus grid in Fig. 5.

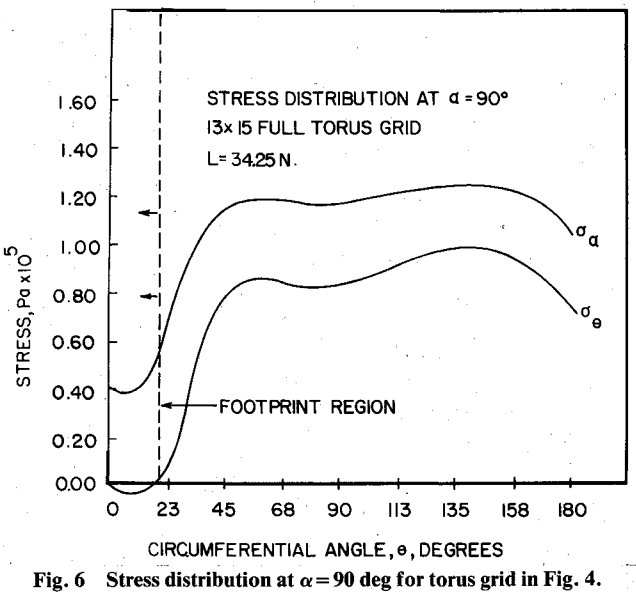

Fig. 6 Stress distribution at $\alpha = 90$ deg for torus grid in Fig. 4.

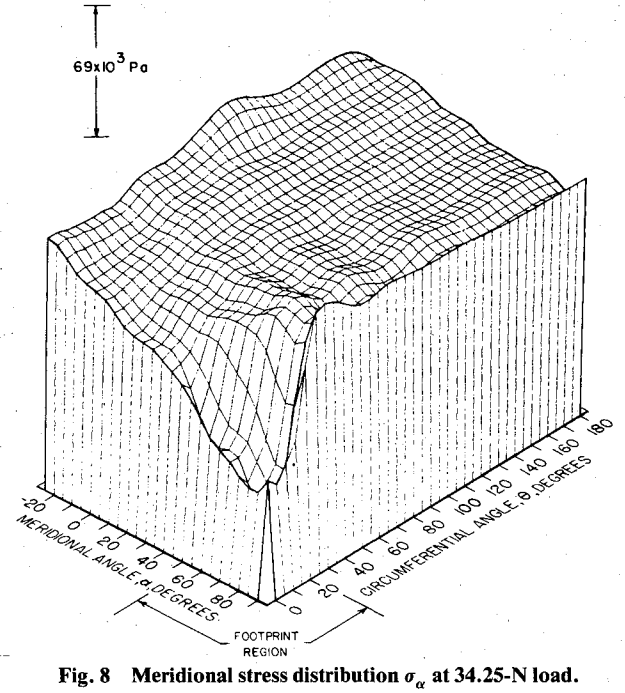

Fig. 8 Meridional stress distribution σ_α at 34.25-N load.

grid from a full torus without increasing the number of degrees of freedom. Figures 4 and 5 show a full and quarter torus, respectively, in both the initial and deformed geometries at a load of 34.25 N. The node density for the torus in Fig. 5 is about four times greater than the torus in Fig. 4 while the number of degrees of freedom is about the same. Note that the contact area approaches a flat plane and the sidewall near the base of the tire exhibits a bulge.

Refining the grid size also has an influence on the stress distributions throughout the torus. Figures 6 and 7 show the stress distributions at $\alpha = 90$ deg, where the angular coordinates α and θ are defined in Fig. 1. Figure 6 shows the stress which results from the grid used in Fig. 4 and Fig. 7 shows the stress which results from the grid used in Fig. 5. The refined grid model allows for a much steeper stress gradient in the footprint region.

Since the grid of Fig. 5 provides reasonable predictions of deflection and stress distribution, as found in Ref. 8, it will be used to consider the influence of increasing load on the torus. Figures 8 and 9 show the meridional and circumferential stress distributions over the surface of the torus for a load of 34.25 N. Even tensile stresses appear in both directions in the upper half of the torus (between θ equal to 90 and 180 deg) as a result of the internal gas pressure. However, the compressive effect of contact with a flat surface reduces these tensile stresses in the footprint region, particularly in the circumferential direction. The circumferential stress is reduced to almost 0 Pa in the center of the footprint region while it remains high in the bulge region (around θ equal to 0 deg and α equal to 5 deg).

At a load of 69.84 N, little change occurs in the stress distribution in the meridional direction. Figure 10 shows the circumferential stress distribution for the 69.84-N load. Note that the compressive effect in the footprint region has increased under increased load so that small compressive stresses exist in the center of the footprint region. As the load continues to increase, this compressive tendency would be expected to continue further.

Figure 11 shows the quarter torus in the initial and deformed configurations under a load of 114.32 N. The deflection of the torus has increased and the degree of bulge in the sidewall is more pronounced under the increased load.

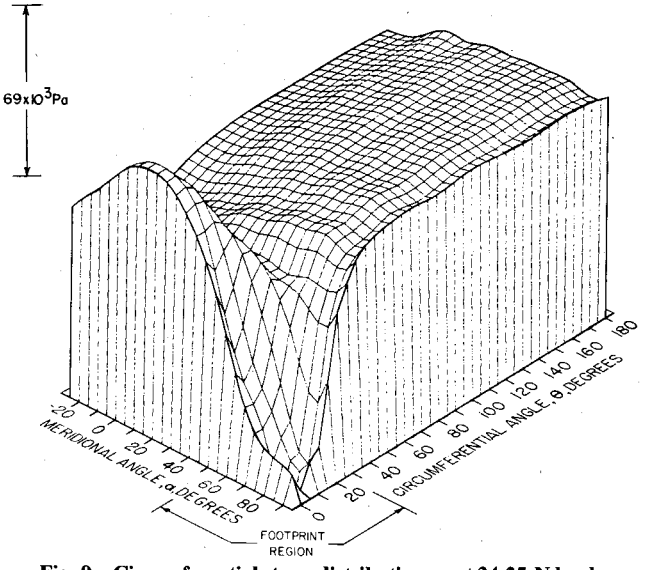

Fig. 9 Circumferential stress distribution σ_θ at 34.25-N load.

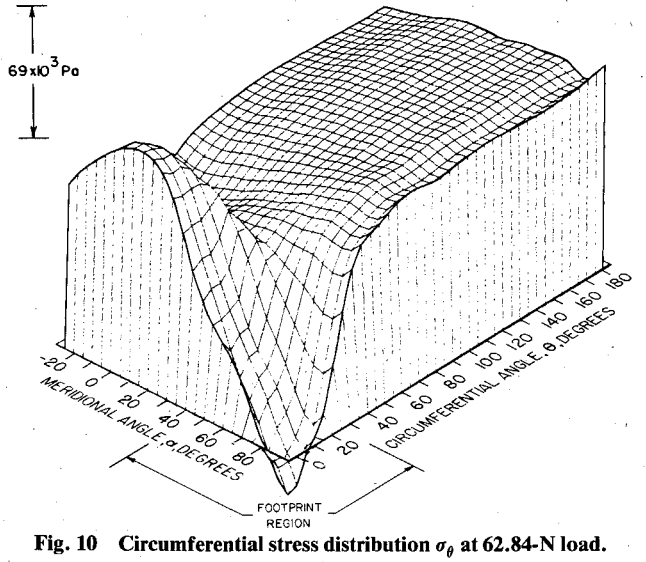

Fig. 10 Circumferential stress distribution σ_θ at 62.84-N load.

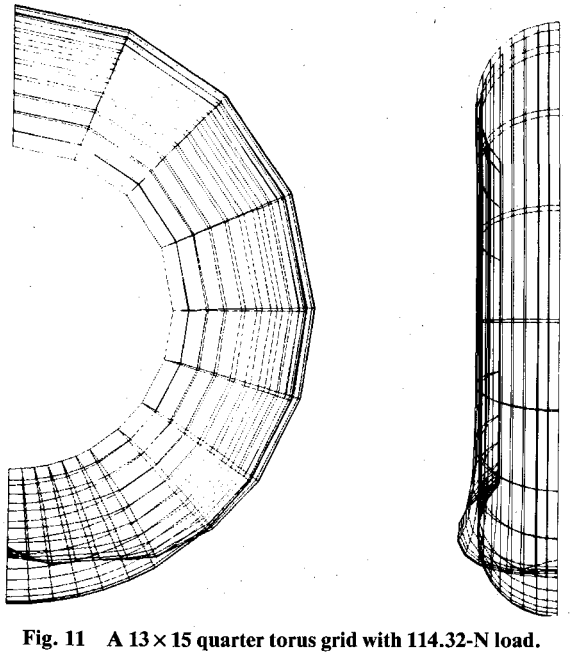

Fig. 11 A 13 × 15 quarter torus grid with 114.32-N load.

Since the elements of the grid have rotated more than 0.3 rad under this loading condition, the results must be interpreted more cautiously. While the accuracy of the results have diminished, the general trends remain valid.

In Fig. 11, the center of footprint region shows negative curvature. This condition is explained by considering the stresses in the footprint region under high load. Figure 12 shows the circumferential stress distribution under a load of 114.32 N. One would expect that loading the torus to 114.32 N would result in an even greater compressive stress in the footprint area. Indeed, Fig. 12 shows that the stress was being reduced and approaching a compressive state near the edges of the footprint. The stress was compressive near the center of the footprint, but then suddenly became tensile again. The erratic stress reversal and shell wall configuration of Fig. 11 suggest that a local limit point on the structural load-deflection path has been reached and snap through has occurred.

The possibility of negative curvature in the center of the footprint under heavy load has some important implications. Generally, the footprint area increases under increasing vertical load. The braking force in a tire is related directly to contact area. The 114.32-N load case suggests that a thin-walled torus under heavy load may have a susceptibility to a local snap through where the contact area actually decreases. It should be noted that any frictional forces between the torus and the contacting surface (which are not modeled here) would tend to reduce a snap-through tendency.

Figure 13 shows the footprint of an inner tube under relatively high load where an initial eccentricity was in-

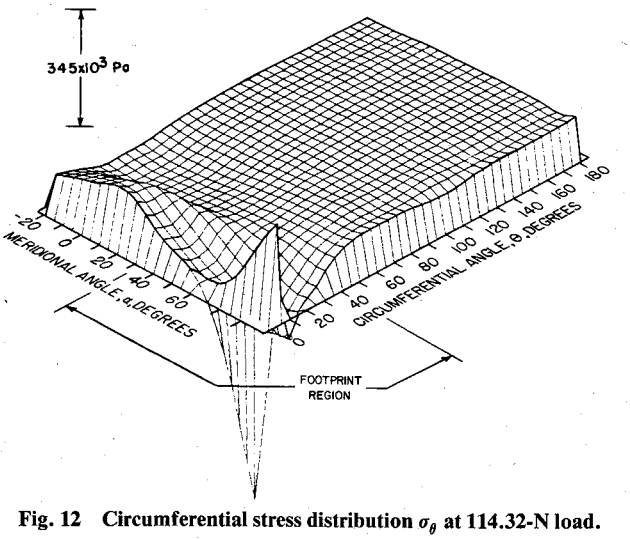

Fig. 12 Circumferential stress distribution σ_θ at 114.32-N load.

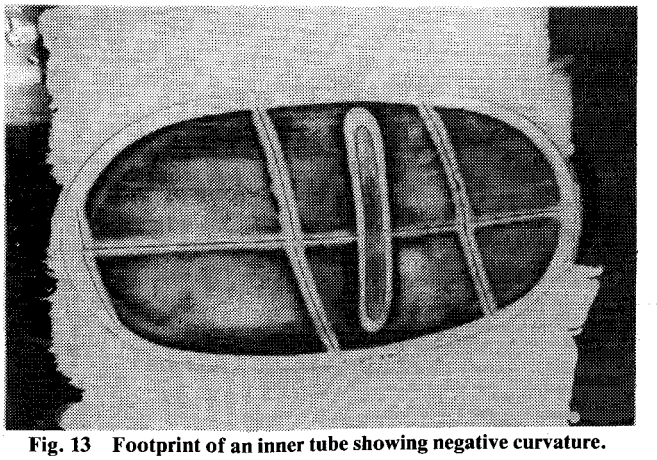

Fig. 13 Footprint of an inner tube showing negative curvature.

troduced into the shell wall. The negative curvature near the center of the footprint might resemble the conditions in a tire under a large load which envelopes a foreign object on the runway.

Conclusions

With the aid of some simplifying assumptions, an analytic model may be derived which predicts deflection and contact area for a thin-walled torus loaded by a plane. The predicted deflection values compare favorably to the measured results at low loads. The assumptions that make the solution of the problem possible also cause the stiffness of the structure to be overestimated.

A finite element program STAGS may be used to predict the deflection and stresses in a torus loaded by a plane. Due to the relatively large deformations and rotations, a nonlinear analysis with incremental loading is necessary for good accuracy. In the case of a static torus, since symmetry exists with respect to two axes, a quarter torus model may be described. This model allows for refining the grid and minimizing the number of degrees of freedom. A grid with smaller elements predicts the deflection, stress distribution, and stiffness of a torus more accurately than a grid with larger elements.

The contact of a torus with a plane reduces the tensile stresses induced by the internal pressure in the region of contact. As the level of external load increases, the circumferential stress in the center of the footprint becomes compressive. As the stress becomes more compressive under a large load, a local limit point may be reached and snap through of the structure occurs. Following snap through, an equilibrium configuration is obtained with negative curvature in the center of the footprint.

Appendix

The vertical height of the center of the torus to the plane in contact may be related as

$$Q=a+b-\delta \tag{A1}$$

The final torus volume is derived as a function of the initial torus dimensions and the deflection by

$$\begin{aligned} V=\pi(a+b)\Big(&(0.5a+b)(4b^2+4ab)^{1/2} \\ &-\frac{(4b^2+4ab)^{3/2}}{3(a+b)}+\frac{(0.5ab+b^2)}{a+b}(4b^2+4ab)^{1/2} \\ &-\frac{(2a^2b+a^3)}{2(a+b)}\ln\left|2(4b^2+4ab)^{1/2}+2a+4b\right|\Big) \\ &-\pi(a+b)\Big(\frac{Q+b}{2}(Q^2+2bQ+b^2-a^2)^{1/2} \\ &-\frac{(Q^2+2bQ+b^2-a^2)^{3/2}}{3(a+b)}+\frac{(bQ+b^2)}{2(a+b)} \\ &\times(Q^2+2bQ+b^2-a^2)^{1/2}-\frac{(2a^2b+a^3)}{2(a+b)}\ln\left|2\right. \\ &\times\left.(Q^2+2bQ+b^2-a^2)^{1/2}+2Q+2b\right|\Big) \end{aligned} \tag{A2}$$

Finally, the torus volume, load, and initial dimensions and pressures are related to the deflection as shown in the following.

$$1-\frac{V=V(a,b,\delta)}{2\pi^2b^2a}\left(\frac{L}{\pi\delta[(2b-\delta)(2a+2b-\delta)]^{1/2}}\right)=(P_i+P_a) \tag{A3}$$

The contact area as a function of deflection and torus dimensions can be derived as

$$A=\pi\delta[(2b-\delta)(2a+2b-\delta)]^{1/2} \tag{A4}$$

Acknowledgments

The authors gratefully acknowledge John A. Tanner, Structure Dynamics Division, NASA Langley for his support and assistance which made this work possible. This research was sponsored by NASA Langley Research Center under NASA Grant 1605 entitled "Load Deflection Characteristics of Inflatable Structures." The Langley Research Center is acknowledged for the use of the computational facilities to perform the STAGS analysis.

References

[1] Smiley, R. F. and Horne, W. B., "Mechanical Properties of Pneumatic Tires with Special Reference to Modern Aircraft Tires," NASA TR R-64, 1960, pp. 7-10.

[2] Clark, S. E., "The Contact between Tire and Roadway," *National Bureau of Standards Monograph* 122, Washington, D.C., 1971, pp. 446-453.

[3] Van Eldik Thieme, H.C.A., "Straight Line Rolling Experiments," *National Bureau of Standards Monograph* 122, Washington, D.C., 1971, p. 569.

[4] DeEskinazi, J., Soedel, W., and Yang, T. Y., "Contact of an Inflated Toroidal Membrane with a Flat Surface as an Approach to the Tire Deflection Problem," *Tire Science and Technology*, TSTCA, Vol. 3, Feb. 1975, pp. 43-61.

[5] Jordan, P. F., "Analytical and Experimental Investigation of Pressurized Toroidal Shells," NASA CR-261, July 1965.

[6] Gassman, P. M., "Deflection and Contact Area of a Standing Torus," M.S. Thesis, Iowa State University, 1980.

[7] Mack, M. J., Jr., "The Finite Element Analysis of an Inflated Toroidal Structure," M.S. Thesis, Iowa State University, 1981.

[8] Hill, D. E., "Experimental Stress Analysis of an Inflated Toroidal Structure," M.S. Thesis, Iowa State University, 1981.